PURPOSE-LED PUBLISHING™

PURPOSE-LED PUBLISHING™

PAPER • **OPEN ACCESS**

Comparison of three dielectric barrier discharges regarding their physical characteristics and influence on the adhesion properties on maple, high density fiberboards and wood plastic composite

To cite this article: F Peters *et al* 2017 *J. Phys. D: Appl. Phys.* **50** 475206

View the article online for updates and enhancements.

You may also like

- Experimental Investigation on Properties of Sugarcane Bagasse Fiberboard Manufactured with Different Techniques
Marianne Nabil Guirguis, Omar Khalaf and Amany Micheal
- Physical and mechanical properties of binderless medium density fiberboard (MDF) from coconut fiber
T Puspaningrum, Y H Haris, I Sailah et al.
- Continuous acoustic separation in a thermoplastic microchannel
A Mueller, A Lever, T V Nguyen et al.

This content was downloaded from IP address 194.95.157.36 on 24/01/2025 at 09:08

OPEN ACCESS
IOP Publishing
Journal of Physics D: Applied Physics
J. Phys. D: Appl. Phys. **51** (2018) 159501 (2pp)
https://doi.org/10.1088/1361-6463/aab378

Corrigendum

Corrigendum: Comparison of three dielectric barrier discharges regarding their physical characteristics and influence on the adhesion properties of maple, high density fiberboard and wood plastic composite (2017 *J. Phys. D: Appl. Phys.* **50** 475206)

F Peters[1,2], B Hünnekens[2], S Wieneke[1], H Militz[2], G Ohms[1] and W Viöl[1,3]

[1] HAWK University of Applied Sciences and Arts, Von-Ossietzky-Straße 100, 37085 Göttingen, Germany
[2] Georg August University of Goettingen, Wood Biology and Wood Products, Burckhardt-Institute, Büsgenweg 4, 37077 Göttingen, Germany
[3] Fraunhofer IST Application Center for Plasma and Photonic, Von-Ossietzky-Straße 100, 37085 Göttingen, Germany

E-mail: wolfgang.vioel@hawk-hhg.de

Received 20 February 2018
Accepted for publication 2 March 2018
Published 20 March 2018

In the article 'Comparison of three dielectric barrier discharges regarding their physical characteristics and influence on the adhesion properties of maple, high density fiberboard and wood plastic composite' (Peters *et al* 2017 *J. Phys. D: Appl. Phys.* **50** 475206) in equation (8), the issue of using the EEPF (electron energy probability function) resulting from the electron Boltzmann equation-solver BOLSIG + is not taken into account. The EEPF, in BOLSIG + called EEDF (electron energy distribution function) or isotropic part of the electron distribution function [1], is defined as the EEDF divided through the root of the energy [2]:

$$f_{\mathrm{EEPF}}(\epsilon) = \frac{f_{\mathrm{EEDF}}(\epsilon)}{\sqrt{\epsilon}}. \tag{1}$$

So, the equation for the rate coefficient taken from [3, 4]

$$k(E/N) \sim \int_0^\infty \sqrt{\epsilon} \cdot \sigma(\epsilon) \cdot f_{\mathrm{EEDF}}(\epsilon, E/N)\, \mathrm{d}\epsilon \tag{2}$$

has to be converted into the one shown in [1, 2, 5]

$$k(E/N) \sim \int_0^\infty \epsilon \cdot \sigma(\epsilon) \cdot f_{\mathrm{EEPF}}(\epsilon, E/N)\, \mathrm{d}\epsilon. \tag{3}$$

The influence on the rate coefficient results in a change of the theoretical ratios of the intensities which leads to a lower resulting reduced electrical field strength and lower mean electron energies and temperatures.

Furthermore, it should be noticed that the values of the reduced electrical field strength, electron energy and

Original content from this work may be used under the terms of the Creative Commons Attribution 3.0 licence. Any further distribution of this work must maintain attribution to the author(s) and the title of the work, journal citation and DOI.

© 2018 IOP Publishing Ltd Printed in the UK

Table 1. Recalculated values for the reduced electric field strengths, mean electron energies and temperatures.

Discharge Type	Material	Reduced electrical field strength (10^{-21} V m^2) [a]	Mean electron energy (eV)	Mean electron temperature (10^3 K)
CSBD	Maple	362 ± 21	8.0 ± 3	62.0 ± 2.4
	HDF	341 ± 21	7.7 ± 3	59.6 ± 2.4
	HDF	341 ± 21	7.7 ± 3	59.6 ± 2.4
	WPC	348 ± 23	7.8 ± 3	60.3 ± 2.6
DDBD	Maple	305 ± 24	7.2 ± 4	55.4 ± 2.9
	HDF	255 ± 18	6.4 ± 3	49.2 ± 2.3
	WPC	387 ± 33	8.4 ± 5	64.8 ± 3.6
RP	Maple	321 ± 27	7.4 ± 4	57.2 ± 3.2
	HDF	316 ± 27	7.3 ± 4	56.7 ± 3.2
	WPC	316 ± 27	7.3 ± 4	56.6 ± 3.2

[a] $1 \cdot 10^{-21}$V m^2 = 1 Td

Table 2. Determined values for the reduced electric field strengths, mean electron energies and temperatures by using emission cross section and equation (4).

Discharge Type	Material	Reduced electrical field strength (10^{-21}V m^2)[a]	Mean electron energy (eV)	Mean electron temperature (10^3 K)
CSBD	Maple	702	12.6	97.4
	HDF	663	12.1	93.4
	WPC	681	12.3	95.2
DDBD	Maple	605	11.3	87.6
	HDF	492	9.8	76.0
	WPC	797	13.8	106.7
RP	Maple	634	11.7	90.5
	HDF	626	11.6	89.7
	WPC	625	11.6	89.6

[a] $1 \cdot 10^{-21}$V m^2 = 1 Td

temperature are relative values and depend on the used data for cross sections and the weighting factors. So, if the emission cross section are used instead of the exciation and ionization cross sections as in [6, 7], equation (20) should be changed into

$$R_{i/j} = \frac{I_i}{I_j} = \left(\frac{\lambda_i}{\lambda_j}\right)^{-1} \frac{g_i}{g_j} \frac{k^i_{\mathrm{em}}}{k^j_{\mathrm{em}}} \tag{4}$$

and the resulting values are higher, about a factor of ≈60% for the temperatures. The emission cross sections can be taken from [8].

Although the absolute values are changed due to the change in the rate coefficient equation, the relative results stay unchanged. There might be a slight dependence on the power but the variations for the DDBD show that does not seem to be the only parameter. So, the change in the rate coefficient does not affect the comparison of the three discharges. Furthermore, the comparision of tables 1 and 2 and the influence of the cross sections show that only comparison of values determined in exactly the same manner is permitted.

Acknowledgements

This work was funded by the Lower Saxony Ministry of Science and Culture and the German Federal Ministry of Education and Research (BMBF), under the supervision of Dr-Ing Karen Otten in Jülich, Germany, and the joint research project "PlaNaWood" (Grant No. 03X5519B).

ORCID iDs

F Peters https://orcid.org/0000-0001-6700-5138
W Viöl https://orcid.org/0000-0003-3425-9937

References

[1] Hagelaar G J M 2016 03.03.2016 Brief documentation of BOLSIG+ version 03/2016 (Université Paul Sabatier, Toulouse, France)
[2] Lieberman M A and Lichtenberg A J 2005 *Principles of Plasma Discharges and Materials Processing* 2nd edn (Hoboken, NJ: Wiley) (https://doi.org/10.1002/0471724254)
[3] Pancheshnyi S 2006 *J. Phys. D: Appl. Phys.* **39** 1708–10
[4] Fantz U 2006 *Plasma Sources Sci. Technol.* **15** S137–47
[5] Hagelaar G J M and Pitchford L C 2005 *Plasma Sources Sci. Technol.* **14** 722–33
[6] Helmke A, Wandke D, Mahmoodzada M, Weltmann K D and Viöl W 2013 *Contrib. Plasma Phys.* **53** 623–38
[7] Hirschberg J, Omairi T, Mertens N, Helmke A, Emmert S and Viöl W 2013 *J. Phys. D: Appl. Phys.* **46** 165201
[8] Itikawa Y 2006 *J. Phys. Chem. Ref. Data* **35** 31–53

OPEN ACCESS
IOP Publishing
Journal of Physics D: Applied Physics
J. Phys. D: Appl. Phys. **50** (2017) 475206 (10pp)
https://doi.org/10.1088/1361-6463/aa8fad

Comparison of three dielectric barrier discharges regarding their physical characteristics and influence on the adhesion properties on maple, high density fiberboards and wood plastic composite

F Peters[1,2], B Hünnekens[2], S Wieneke[1], H Militz[2], G Ohms[1] and W Viöl[1,3]

[1] HAWK University of Applied Sciences and Arts, Von-Ossietzky-Straße 100, 37085 Göttingen, Germany
[2] Georg August University of Goettingen, Wood Biology and Wood Products, Burckhardt-Institute, Büsgenweg 4, 37077 Göttingen, Germany
[3] Fraunhofer IST Application Center for Plasma and Photonic, Von-Ossietzky-Straße 100, 37085 Göttingen, Germany

E-mail: wolfgang.vioel@hawk-hhg.de

Received 26 June 2017, revised 15 September 2017
Accepted for publication 28 September 2017
Published 3 November 2017

Abstract

In this study, three different dielectric barrier discharges, based on the same setup and run with the same power supply, are characterized by emission spectroscopy with regards to the reduced electrical field strength, and the rotational, vibrational and electron temperature. To compare discharges common for the treatment on wood, a coplanar surface barrier discharge, a direct dielectric barrier discharge and a jet system/remote plasma are chosen. To minimize influences due to the setups or power, the discharges are realized with the same electrodes and power supply and normalized to the same power. To evaluate the efficiency of the different discharges and the influence on treated materials, the surface free energy is determined on a maple wood, high density fiberboard and wood plastic composite. The influence is measured depending on the treatment time, with the highest impact in the time of 5 s.

Keywords: dielectric barrier discharge, low temperature plasma, emission spectroscopy, surface free energy, wood

(Some figures may appear in colour only in the online journal)

1. Introduction

For several application fields and materials, plasma treatment is used for surface activation in order to enhance adhesion properties. Particularly for the treatment of polymers, extensive research has been done in the past [1–4]. In recent years, natural materials such as wood and wood-based materials, have become increasingly relevant in this field. Wood is the most common building material and combines several advantages, such as comparatively low cost, renewable and sustainable production, carbon capture and storage potential, as well as a balanced relation of weight and mechanical strength [5].

The plasma treatment of wood and wooden materials is still in its beginning stages although the first patents have existed for more than 15 years [6]. Often, surfaces are treated or coated by low pressure plasma discharges. Atmospheric

Original content from this work may be used under the terms of the Creative Commons Attribution 3.0 licence. Any further distribution of this work must maintain attribution to the author(s) and the title of the work, journal citation and DOI.

pressure plasma treatment on wood is preferable to low pressure treatment, due to the much simpler handling. Wood as a natural material has some properties which might cause problems in several applicactions. Its hygroscopicity enables the wood to absorb moisture, which leads to swelling, whereas the drying of wood causes shrinkage of the material. Therefore, the dimensions are not stable and strongly dependent on the relative humidity of the ambient air. Moreover, many wood species have low natural durability; weathering and biological attacks by fungi and insects affect the appearance and mechanical properties negatively and result in material degradation [7–9]. Both the treatments necessary for increasing the durability as well as the production of wooden materials can be improved significantly by a plasma treatment [10–13]. Plasma is applied to wood and wooden surfaces to enhance the wetting properties for further improvement of the surface and composite properties in various applications. It is known to improve adhesion, leading to better bonding performance of the materials [14–17].

Still, the plasma treatment of wood and wooden materials needs further investigation. For these materials, dielectric barrier discharges are the most commonly used plasma sources, due to their low thermal impact. This study compares three kinds of plasma discharges, using normal air as the process gas, with regards to their temperatures. Cold, non-equilibrium plasmas are defined by their electron temperature T_e, their vibrational temperature T_{vib}, as well as by their rotational temperature T_{rot} and their translational temperature T_{trans}, which is equivalent to the gas temperature T_{gas}. The rotational temperature corresponds to the gas temperature, while the electrons and vibrationally exited species are chemically reactive [18]. All of these temperatures are mean temperatures, since the temperatures in plasma are defined by distributions. The efficiency of the plasma treatment and the used plasma sources is presently evaluated by surface energy measurements.

A setup was built which can be used for the three discharge types: a coplanar surface barrier discharge (CSBD), a direct dielectric barrier discharge (DDBD) and a remote plasma configuration (RP) [19]. For better comparability, all three configurations are connected to the same power supply and normed to the same power, but are still dependent on the used material.

The treatment is applied to three different materials, taken as examples for wood and wooden materials: maple (*Acer spec.*), high density fiberboard (HDF) and wood plastic composite (WPC). Fiberboards are often covered by veneers or décor papers, so improving the gluing process is of interest to a large commercial market. The market for WPC is growing, especially for outdoor applications. Due to the UV of sunlight, the WPC changes its color. Coatings usually have a low adhesive strength on a WPC. Thus, an improvement of the adhesion behavior finds its application here as well.

2. Setup

All three plasma setups were based on the principle of the dielectric barrier discharge (DBD) and realized by the same two 250 mm-long electrodes. The bronze electrodes were covered with a dielectric material, Al_2O_3 ceramic, of 2.5 mm thickness and cooled inside with an air flow. As the process gas, normal air (120 l min^{-1}) was streamed into the discharges between the electrodes. The different setups were created by different wirings and placements. Diagrams of the three kinds of setup are shown in figures 1–3. For visualisation, pictures of the discharges were taken by a Nikon D90 camera (Nikon Corporation, Tokyo, Japan) and are shown in figures 4–6. The coplanar surface barrier discharge (CSBD, figure 1) had one electrode on high voltage, the other one grounded and both separated by an additional glass barrier of 3 mm thickness. The distance to the samples was approx. 0.5 mm. The second configuration, the direct dielectric barrier discharge (DDBD, figure 2), had two electrodes connected to the high voltage and an additional with a 4 mm glass covered, grounded electrode below the sample. The distances between both the high voltage electrodes and to the sample were 2 mm. The third configuration was the remote plasma (RP, figure 3) setup with one grounded electrode and one which was connected to the high voltage. The distances, the inter-electrode distance as well as the electrode-sample distance, were the same as for the DDBD. For all configurations, the applied power supply was pulsed with a frequency of 15 kHz with alternating pulses of 27 µs duration. The high voltage ranges from 19 kV to 29 kV (table 4). To lower the thermal impact, 1 s of plasma treatment was followed by an interval of 1 s.

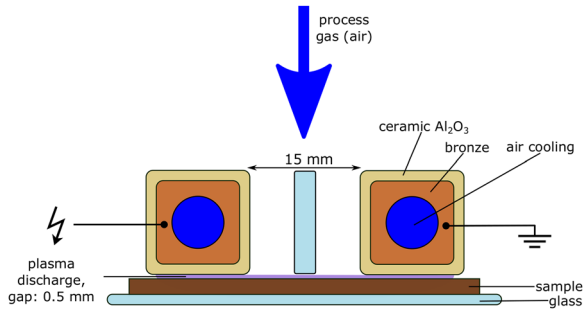

Figure 1. Coplanar surface barrier discharge (CSBD), modified after [19]. [19] John Wiley & Sons. © 2016 Wiley Periodicals, Inc.

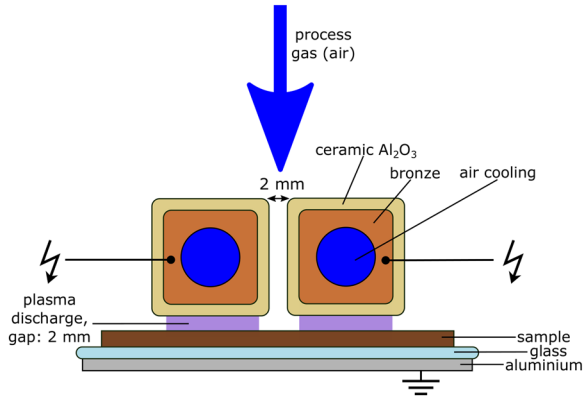

Figure 2. Direct dielectric barrier discharge (DDBD), modified after [19]. [19] John Wiley & Sons. © 2016 Wiley Periodicals, Inc.

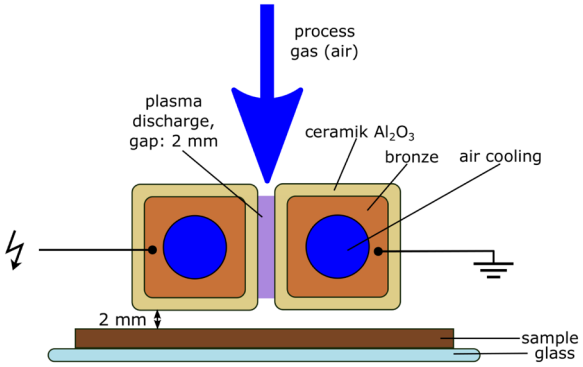

Figure 3. Remote plasma/jet configuration (RP), modified after [19]. [19] John Wiley & Sons. © 2016 Wiley Periodicals, Inc.

Table 1. Volumetric mass density.

	Mass density (kg m^{-3})
Maple	633.6 ± 3.7
HDF	836.1 ± 10.9
WPC	1154.1 ± 9.5

3. Materials and methods

3.1. Materials

The impact of plasma treatment and the physical parameters resulting from the interaction between the plasma discharge and the substrate were analyzed based on three different types of wood and wood-based materials: solid wood of maple (*Acer spec.*), wood-polymer composites (WPC) and high density fiberboard (HDF). The densities are shown in table 1. On maple, the tests were performed on the radial surface. The HDF used in this study was a commercial product. The WPC was manufactured by an extrusion process in a parallel twin-screw extruder (ZSE 27 IMAXX-40D, Leistritz AG, Nürnberg, Germany). The content of the composite was 60.9 wt% softwood (Arbocel®C 100, Rettenmaier & Söhne GmbH und Co. KG, Rosenberg, Germany) and 39.1% PP (SABIC 575 P, Saudi Basic Industries Corparation, Riyadh, Saudi Arabia) with a melt flow rate (MFR) at 503 K and a 2.16 kg load of 1.1 g min^{-1}. A coupling agent (Licocene PP MA 6452 granulate TP, Clariant International Ltd., Muttenz, Switzerland) was added (3 wt% based on the weight of wood and PP). To determine the surface free energy, all of the samples were cut to size with dimensions of $100 \times 50 \times 4$ mm^3. For the other measurements, a sample size of $250 \times 50 \times 4$ mm^3 was used. Prior to testing, the samples were stored in a climate chamber at 20 °C/65% RH for two weeks.

3.2. Power measurement

To measure the electrical power, a high voltage probe (PVM-1, North Star High Voltage, Bainbridge Island, USA) with 13 pF and 400 MΩ was connected to the power supply. Two capacitors ($2 \cdot C_m = 200$ nF) and a resistance of $R_m = 1$ kΩ were added to the circuit before grounding. At three locations, the voltage was measured with an oscilloscope (DL1740EL,

Figure 4. Coplanar surface barrier discharge (CSBD), exposure time: 1/3 s.

Figure 5. Direct dielectric barrier discharge (DDBD), exposure time: 1 s.

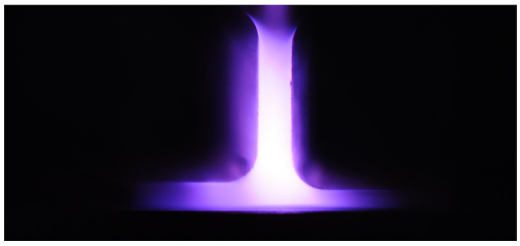

Figure 6. Remote plasma/jet configuration (RP), exposure time: 1/10 s.

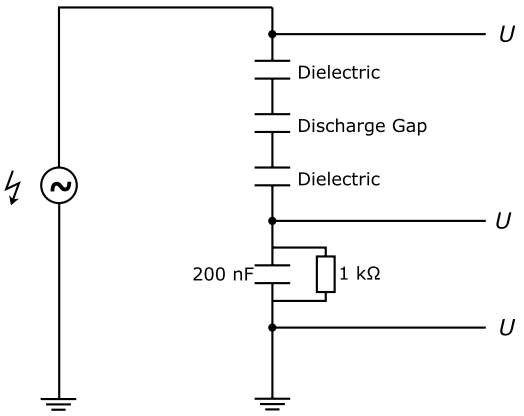

Figure 7. Equivalent circuit diagram for the power measurement.

Yokogawa Electric Corp., Musashino, Japan): at the high voltage probe (U_{total}), behind the grounded electrode (U_{m1}), and behind the added capacitors and the resistance (U_{m2}) to negate the influence of induced voltages inside the wiring due to the applied high frequency alternating voltage. The equivalent circuit diagram for the power measurement can be seen in figure 7. The instantaneous energy E can be estimated by the following equation:

$$E = U_{total} \cdot C_m \cdot (U_{m1} - U_{m2}). \quad (1)$$

The mean power $\overline{P}$ can be determined by the integration of the Lissajous figure multiplied by the pulse repetition frequency f:

$$\overline{P} = f \cdot C_{\mathrm{m}} \cdot \oint (U_{\mathrm{m1}} - U_{\mathrm{m2}})\, \mathrm{d}U_{\mathrm{total}}. \tag{2}$$

3.3. Surface temperature measurements by infrared imaging

The maximum surface temperature was measured after 30 s of plasma treatment. Therefore, the samples were removed after the plasma treatment from the discharge and a video with 1 frame per second was taken with an infrared camera (VarioCam hr research, InfraTec GmbH, Dresden, Germany). With these measurements, the treated area and the maximum surface temperature were evaluated. The treated area is used to approximate the power surface density.

3.4. Temperature measurements by emission spectroscopy

The temperatures inside the plasma discharge were determined by emission spectroscopy with the echelle spectrometer Aryelle-Butterfly 400 (LTB Lasertechnik Berlin GmbH, Berlin, Germany). The spectrometer was calibrated to the wavelength and relative intensity. The optical fiber was placed vertical to the slit between the electrode, so that the light from the whole discharge could be collected. The integration time for all three discharges and samples was 3 min, with a plasma time of 90 s.

3.4.1. Rotational temperature. At atmospheric pressure, the gas temperature (translational temperature) can be approximated by the rotational temperature, due to the fast rotational-to-translational relaxation [20, 21]. The rotational temperatures were determined by comparing the measured spectra to a database of simulated ones with a Matlab routine (MATLAB R2015b, The MathWorks GmbH, Ismaning, Germany) using the least-squares-method. The simulated spectra were generated by the software Specair 3.0 (SpectralFit, Antony, France), which is a common software to simulate plasma spectra. The spectra were compared in the wavelength ranges of 334 nm to 337.2 nm and 360 nm to 382 nm, the rotational branches of the second positive system of nitrogen $\mathrm{N_2}(C^3\Pi_{\mathrm{u}} - B^3\Pi_{\mathrm{g}})$ for vibrational band $v = 0 - 0$ and the vibrational band sequence with $\Delta v = -2$.

3.4.2. Vibrational temperature. The vibrational temperature T_{vib} was determined by the Boltzmann plot method. Therefore, the energy of the upper levels E was calculated with the equation [22]

$$E(v', J = 0) = T_{00} + G(v'), \text{ with} \tag{3}$$

$$G(v') = \omega_e(v' + \frac{1}{2}) - \omega_e\chi_e(v' + \frac{1}{2})^2. \tag{4}$$

The molecular constants for this nitrogen system, T_{00}, ω_e and $\omega_e\chi_e$, were taken from [23]. For nitrogen as a diatomic molecule, the statistic weight g is one [24], so for the Boltzmann plot method, $\ln\left(I_{v'v''} \cdot \lambda_{v'v''} \cdot A^{-1}_{v'v''}\right)$ is plotted over the upper level energy in eV. The temperature is

$$T_{\mathrm{vib}} = -\frac{\Delta E}{\Delta \ln\left(I_{v'v''} \cdot \lambda_{v'v''} \cdot A^{-1}_{v'v''}\right)} \cdot k_{\mathrm{B}}^{-1}. \tag{5}$$

The Einstein coefficients $A_{v'v''}$ were obtained from [25]. The intensities were in the range of 300 nm to 400 nm with the upper vibrational numbers of $v = 0$ to $v = 4$. The error of the vibrational temperature was determined by the propagation of the slope error.

3.5. Electrical field strength and mean electron energy

The emission spectra measurements with the Aryelle-Butterfly 400 were used for the electrical field strength determination as well. This method was taken from [26–28]. Therefore, three nitrogen transitions of the second positive system (SPS) were considered:

(i) $\mathrm{N_2}(C^3\Pi_u, v = 0) \rightarrow \mathrm{N_2}(B^3\Pi_g, v = 0)$ (SPS(0,0)) at $\lambda = 337.1$ nm,
(ii) $\mathrm{N_2}(C^3\Pi_u, v = 0) \rightarrow \mathrm{N_2}(B^3\Pi_g, v = 1)$ (SPS(0,1)) at $\lambda = 357.6$ nm and
(iii) $\mathrm{N_2}(C^3\Pi_u, v = 0) \rightarrow \mathrm{N_2}(B^3\Pi_g, v = 2)$ (SPS(0,2)) at $\lambda = 380.4$ nm.

These transitions were set in relation to the transition of the first negative system (FNS) $\mathrm{N_2^+}(B^2\Sigma_g^+, v = 0) \rightarrow \mathrm{N_2^+}(X^2\Sigma_g^+, v = 0)$ (FNS(0,0)) at $\lambda = 391.4$ nm. The ratios of the corresponding measured peak intensities were compared to the theoretically calculated values dependent on the reduced electrical field strength (E/N). For a low degree of vibrational excitation, the population of these two upper nitrogen levels, $\mathrm{N_2}(C^3\Pi_u, v = 0)$ and $\mathrm{N_2^+}(B^2\Sigma_g^+, v = 0)$, is related to an electron-impact excitation from the ground state of nitrogen:

$$\mathrm{N_2}(X^1\Sigma_g^+, v = 0) + \mathrm{e} \xrightarrow{k_{\mathrm{ex,\ N_2}(C^3\Pi_u, v=0)}} \mathrm{N_2}(C^3\Pi_u, v = 0) + \mathrm{e} \tag{6}$$

$$\xrightarrow{k_{\mathrm{ex,\ N_2^+}(B^2\Sigma_g^+, v=0)}} \mathrm{N_2^+}(B^2\Sigma_g^+, v = 0) + \mathrm{e} + \mathrm{e}. \tag{7}$$

The excitation rate coefficient was calculated by the following equation with the cross sections and the electron energy probability function (EEPF) $f(\epsilon)$

$$k_{\mathrm{ex}}(E/N) \sim \int_0^\infty \sqrt{\epsilon}\sigma_{\mathrm{ex}}(\epsilon) \cdot f(\epsilon, E/N)\, \mathrm{d}\epsilon. \tag{8}$$

The distribution function was normalized [27, 29]

$$\int_0^\infty f(\epsilon)\sqrt{\epsilon}\, \mathrm{d}\epsilon = 1. \tag{9}$$

The excitation and ionisation cross sections for the rate coefficient were taken from [30]. The EEPF was simulated for the E/N-range from 100 Td to 1000 Td with the electron Boltzmann equation-solver Bolsig+ (03/2016) [29] and the cross section data for nitrogen and oxygen of LXcat with the database IST-Lisbon [31]. The ionisation degree was estimated as 10^{-6} and the electron density as 2.5×10^{19} $\mathrm{m^{-3}}$.

Table 2. Constants for the weighting factors of $N_2(C^3\Pi_u, v=0)$ and $N_2^+(B^2\Sigma_u^+, v=0)$ [27, 33, 34].

		$N_2(C^3\Pi_u, v=0)$	$N_2^+(B^2\Sigma_u^+, v=0)$
τ_0	(10^{-9} s)	42	62
k_{q,N_2}	(10^{-10} cm^3 s^{-1})	0.13	2.1
k_{q,O_2}	(10^{-10} cm^3 s^{-1})	3.0	5.1
k_{conv}	(10^{-29} cm^6 s^{-1})	—	5.0

Taking the following relaxation mechanism of $N_2(C^3\Pi_u, v=0)$ and $N_2^+(B^2\Sigma_u^+, v=0)$ into account,

(i) radiative transitions

$$N_2(C^3\Pi_u, v=0) \xrightarrow{\tau_{0,SPS}^{-1}} N_2(B^3\Pi_g, v=0) + h\nu_{337} \quad (10)$$

$$\xrightarrow{\tau_{0,SPS}^{-1}} N_2(B^3\Pi_g, v=1) + h\nu_{357} \quad (11)$$

$$\xrightarrow{\tau_{0,SPS}^{-1}} N_2(B^3\Pi_g, v=2) + h\nu_{380} \quad (12)$$

$$N_2^+(B^2\Sigma_u^+, v=0) \xrightarrow{\tau_{0,FNS}^{-1}} N_2^+(X^2\Sigma_g^+, v=0) + h\nu_{391}, \quad (13)$$

(ii) quenching by collisions with heavy particles as N_2 or O_2

$$N_2(C^3\Pi_u) + M \xrightarrow{k_{q,SPS}} \text{products} \quad (14)$$

$$N_2^+(B^2\Sigma_u^+) + M \xrightarrow{k_{q,FNS}} \text{products}, \quad (15)$$

(iii) as well as the associative attachment, due to the filamented character of the discharge

$$N_2^+(B^2\Sigma_u^+) + N_2 + M \xrightarrow{k_{conv}} N_4^+ + M, \quad (16)$$

corresponding weighting factors g, fractions of radiating molecules, can be determined by

$$g_{SPS} = C^{-1} \quad \text{and} \quad (17)$$

$$g_{FNS} = \left(C + \tau_{0,FNS} k_{conv} n_{N_2} N^2\right)^{-1} \quad (18)$$

with

$$C = 1 + \tau_0 \left(n_{N_2} k_{q,N_2} + n_{O_2} k_{q,O_2}\right) N. \quad (19)$$

The data for the weighting factors are listed in table 2. With the wavelength of the transitions λ, the corresponding transition probability $A_{vib,v'v''}$, the excitation rate coefficients k_{ex}, and the weighting factor g, a theoretical ratio R dependent on the electrical field strength could be determined:

$$R_{i/j} = \frac{I_i}{I_j} = \left(\frac{\lambda_i}{\lambda_j}\right)^{-1} \frac{A^i_{vib,v'v''}}{A^j_{vib,v'v''}} \frac{g_i}{g_j} \frac{k^i_{ex}}{k^j_{ex}}. \quad (20)$$

The transition probability is defined by the Franck–Condon factors q and the wavenumber ν in cm^{-1} [32]:

Table 3. Surface tension data for the five liquids used [35].

Liquid	CAS#	Surface tension (mN m^{-1})	
		Dispers	Polar
Water	7732-18-5	21.8	51.0
Ethylene Glycol	107–21–1	31.4	16.4
Glycerol	56–81–5	34.4	29.5
Bromonaphthalene	90–11–9	44.4	—
Diiodomethane	75–11–6	50.8	—

$$A_{vib,v'v''} = \frac{q_{v'v''}\nu^3_{v'v''}}{\sum_v q_{v'v''}\nu^3_{v'v''}}. \quad (21)$$

The Franck–Condon factors q were taken from [25]. The theoretically determined ratio as function of E/N is interpolated. By this function, the measured ratio is transferred into a reduced electrical field strength E/N. With Bolsig+, the reduced electric field strength can be converted into a mean electron energy and therefore a mean electron temperature. The resulting data from the ratios $R_{391/337}$, $R_{391/357}$ and $R_{391/380}$ were averaged.

3.6. Optical fiber thermometer measurements

The gas temperature inside the plasma was determined with a fiber optic temperature sensor, FOT-L-SD (FISO Technologies Inc., Québec, Canada) and a UMI4 (Universal Multichannel Instrument, FISO Technologies Inc., Québec, Canada). Due to the maximum treatment time, as well as the integration time of the emission spectroscopy, the temperatures were measured after 30 s and 90 s.

3.7. Contact angles and surface free energy

The contact angles required for determining the surface free energy were measured using the system KRÜSS GS 10 (KRÜSS GmbH, Hamburg, Germany) with the corresponding software KRÜSS DSA 1.80. The sessile drop method with the advancing contact angles was chosen. Therefore, for each measurement point, a 10 s-video with 25 frames per second was taken. The contact angle videos taken with the GS 10 were converted into data with the software DSA1 and the circle fitting method. With a Matlab routine, the following data analysis was done. Due to the advancing and scattering behavior of the contact angles especially on wood, the decreasing values were smoothed by applying an exponential fit with the function $\Theta(t) = a \cdot \exp(-b \cdot t) + c \cdot t^2 + d \cdot t + e$. In this study, the contact angle was defined as the value of this function at the time $t = 0.4$ s as the point after the settling behavior of the drops and before an increasing soaking into the material. The resulting contact angle data for the five liquids (liquid surface tension data shown in table 3) were used as input for the Fowkes model of surface free energy determination. The Fowkes theory is mathematically equivalent to that

Table 4. Mean electrical power, surface power density and maximum voltage of the discharges, depending on the used material for different discharge types.

Discharge type	Material	Mean electrical power (W)	Power/area (W cm^{-2})	Maximum voltage (kV)
CSBD	Maple	192 ± 10	3.03 ± 0.16	28.49 ± 0.19
	HDF	185 ± 10	4.09 ± 0.22	28.38 ± 0.06
	WPC	175 ± 9	3.10 ± 0.16	28.38 ± 0.10
DDBD	Maple	147 ± 7	1.57 ± 0.07	24.16 ± 0.00
	HDF	127 ± 4	1.42 ± 0.04	24.50 ± 0.05
	WPC	144 ± 5	1.52 ± 0.05	24.11 ± 0.10
RP	Maple	149 ± 5	1.65 ± 0.06	19.34 ± 0.18
	HDF	149 ± 4	1.70 ± 0.05	19.30 ± 0.12
	WPC	155 ± 5	1.67 ± 0.05	19.58 ± 0.00

of Owens–Wendt–Rabel [36]. All of the surface free energy theories are based on the Young equation [37]:

$$\sigma_S = \sigma_{SL} + \sigma_L \cos\Theta \tag{22}$$

with σ_S as the overall surface energy of the solid, σ_L as the overall surface tension of the wetting liquid, σ_{SL} as the interfacial tension between the solid and the liquid and Θ as the contact angle between the liquid and the solid. The different surface free energy theories describe the interaction between the solid and the liquid, σ_{SL}. The Fowkes theory separates the interaction into a dispersive component and a non-dispersive (polar) component:

$$W_{SL} = 2\left(\sqrt{\sigma_L^D \cdot \sigma_S^D} + \sqrt{\sigma_L^P \cdot \sigma_S^P}\right). \tag{23}$$

Here, W_{SL} is the work of adhesion per area between the liquid and the solid, σ_L^D the dispersive component of the liquid surface tension, σ_L^P the polar component of the liquid surface tension, and σ_S^D and σ_S^P consequently the dispersive and polar components of the solid surface energy. As a combination of these two equations with the Dupre definition of the adhesion work ($W_{SL} = \sigma_S + \sigma_L - \sigma_{SL}$), the fundamental equation of Fowkes theory results in:

$$\frac{1}{2}\sigma_L(\cos\Theta + 1) = \sqrt{\sigma_L^D \cdot \sigma_S^D} + \sqrt{\sigma_L^P \cdot \sigma_S^P}. \tag{24}$$

As a first step, this equation was solved for only the dispersive liquids with $\sigma_L^P = 0$ and therefore $\sigma_L^D = \sigma_L$. This simplified the equation to

$$\cos\Theta = 2\sqrt{\sigma_S^D} \cdot \left(\sqrt{\sigma_L^D}\right)^{-1} - 1. \tag{25}$$

σ_S^D is determined by plotting $\cos\Theta$ against $\left(\sqrt{\sigma_L^D}\right)^{-1}$ for bromonaphthalene and diiodomethane and processing a linear regression with the interception of 10^{-1}. The slope was converted into the dispersive component of the solid surface energy. With the resulting σ_S^D, the contact angle data of the other liquids were calculated into $W_{SL}^P = \sigma_L(\cos\Theta + 1) - 2\sqrt{\sigma_L^D \cdot \sigma_S^D}$ and plotted against $2\sqrt{\sigma_L^P}$. The linear regression had to have an interception of 0. This second slope was transferred into the polar component of the solid surface energy σ_S^P. The errors of the calculated surface energies derived by error propagation from the errors of the slopes with a confidence interval of 70%. These plots, fits and calculations were done in the Matlab R2015b as well.

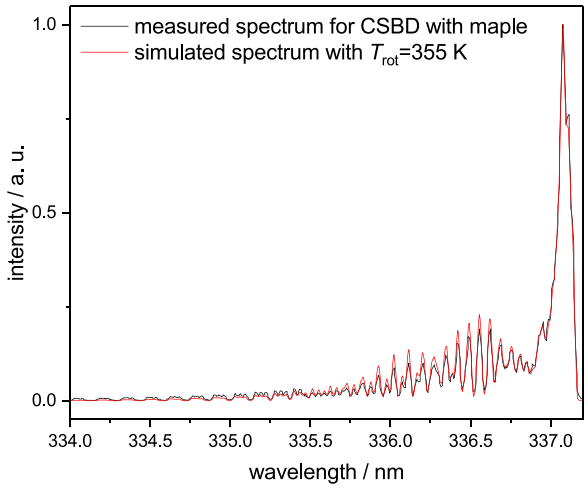

Figure 8. Measured and simulated spectra of $N_2(C^3\Pi_u - B^3\Pi_g, v = 0 - 0)$ for CSBD with maple.

4. Results and discussion

4.1. Electrical power

The measured electrical properties are listed in table 4. Due to the power supply, which can only be regulated by the voltage amplitude, the resulting powers depend on using material beside the RP. The highest sensitivity to material changes was seen with the CSBD. Here, the different electrical conductivities of the materials have a high influence. With the assumption $M_{Maple} > M_{HDF} > M_{WPC}$ for the moisture content M, the power dependence of CSBD can be explained. For the DDBD, different powers were measured as well. The samples work here as an additional dielectric material and influence the discharge. For both the CSBD and the DDBD, no significant relation between the measured powers and the material density was shown. The RP with the smallest variation is independent on the sample material, due to the jet configuration.

Table 5. Rotational temperatures, determined by comparison with simulated spectra (Specair), gas temperatures after 30 s and 90 s of plasma treatment time, and the surface temperatures.

Discharge type	Material	T_{rot} (K)		T_{gas} (K)		$T_{surface}$ (K)
		$v = 0 - 0$	$\Delta v = -2$	$t_P = 30$ s	$t_P = 90$ s	
CSBD	Maple	355	420	349	367	315.4 ± 2.6
	HDF	340	440	335	337	
	WPC	315	340	333	343	
DDBD	Maple	390	460	330	340	310.4 ± 1.8
	HDF	370	340	322	326	
	WPC	310	365	322	330	
RP	Maple	310	400	311	312	300.7 ± 0.4
	HDF	310	400	306	308	
	WPC	310	400	308	309	

4.2. Surface temperatures

For the surface temperature $T_{surface}$, the maximum value resulting from a 30 s plasma treatment was below 318 K. The temperatures were dependent on the discharge types but not significantly on the surface material. Thus, the highest temperature was measured for the CSBD (315.4 K $\pm$ 2.6 K) and the lowest for the RP (300.7 K $\pm$ 0.4 K). The CSBD temperatures can be explained by the application of the electrical power on a smaller area, while the distance between the RP and the sample surface leads to a cooling of the plasma species. The DDBD lay in between, with a temperature of 310.4 K $\pm$ 1.8 K. Thus, a 30 s plasma treatment leads to only a small increase of the surface temperature, still comparable to the room temperature. A thermal degeneration of the materials by a plasma treatment as presented is highly unlikely.

4.3. Rotational and gas temperature

Figure 8 shows the spectrum of $N_2(C^3\Pi_u - B^3\Pi_g, v = 0 - 0)$ with the corresponding rotational bands measured for the CSBD on maple with the best fitting simulated spectrum. The other temperatures are listed in table 5, together with the gas temperatures determined by the optical fiber temperature measurements. With regards to the maximum plasma treatment time and the integration time of the emission spectroscopy measurements, the gas temperatures after 30 s and 90 s were measured. In this way, the temperatures after 90 s can be compared with the rotational temperatures. Since the rotational temperature determination with Specair in the wavelength range of 360 nm to 382 nm ($N_2(C^3\Pi_u - B^3\Pi_g)$, vibrational band squence with $\Delta v = -2$) has an error of up to $\pm$50 K [38], the accuracy of the determination is assumed to be $\pm$100 K as the maximum difference between both methods to determine T_{rot}.

For the CSBD and RP, the values of T_{rot} of the $v = 0 - 0$ peak especially match very well with the T_{gas}. The difference for the DDBD might be explained by the small measurement area of the optical fiber thermometer so that the measurement was not performed at the hottest area. For the emission spectroscopy measurements of the T_{rot}, areas with a higher temperature can dominate the emitted light and heighten the measured temperatures. Nevertheless, the method works very well for determining of T_{gas} without disturbing the discharge. Of all three discharge types, WPC shows the lowest T_{rot}. This cannot be seen so clearly for T_{gas}. The RP is characterized by the lowest temperatures for T_{rot} of the $v = 0 - 0$ peak inside the plasma, as well as for T_{gas} between plasma and surface. The RP also shows the smallest variation of the temperatures between the materials; proof together with the power data for the independence from the materials.

Table 6. Vibrational temperatures determined by Boltzmann plot together with the coefficient of determination R^2.

Discharge type	Material	T_{vib} (K)	R^2
CSBD	Maple	2447 ± 245	0.96
	HDF	2387 ± 252	0.95
	WPC	2375 ± 223	0.96
DDBD	Maple	2655 ± 307	0.94
	HDF	2576 ± 291	0.94
	WPC	2533 ± 291	0.94
RP	Maple	2474 ± 300	0.94
	HDF	2500 ± 264	0.95
	WPC	2444 ± 258	0.95

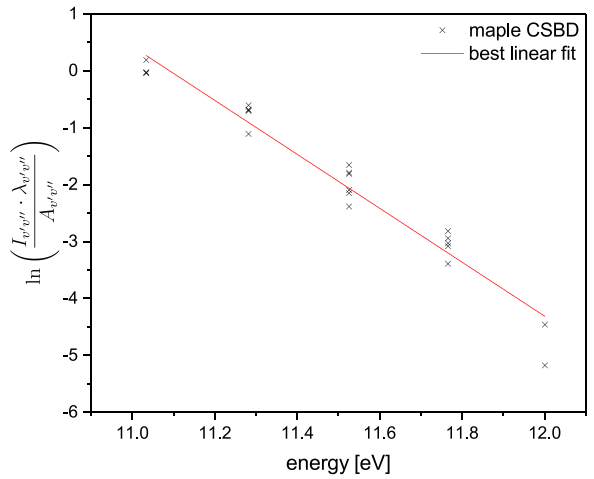

Figure 9. Vibrational Boltzmann plot for CSBD with maple.

Table 7. Determined reduced electric field strengths, mean electron energies and temperatures for different discharge types.

Discharge type	Material	Reduced electrical field strength $(1 \cdot 10^{-21}$ V m$^2)$[a]	Mean electron energy (eV)	Mean electron temperature (10^3 K)
CSBD	Maple	420 ± 21	8.8 ± 0.3	68.4 ± 2.2
	HDF	391 ± 29	8.4 ± 0.4	65.2 ± 3.1
	WPC	395 ± 26	8.5 ± 0.4	65.6 ± 2.9
DDBD	Maple	355 ± 24	7.9 ± 0.3	61.2 ± 2.7
	HDF	296 ± 25	7.0 ± 0.4	54.3 ± 3.0
	WPC	437 ± 40	9.1 ± 0.5	70.2 ± 4.2
RP	Maple	361 ± 0.31	8.0 ± 0.5	61.8 ± 3.5
	HDF	353 ± 29	7.9 ± 0.4	61.0 ± 3.3
	WPC	354 ± 31	7.9 ± 0.5	61.1 ± 3.5

[a] $1 \cdot 10^{-21}$ V m^2 = 1 Td.

Table 8. Error estimation, due to the error propagation of the Fowkes model.

Liquid	Range of Θ (°)		max ΔΘ (°)	max. est. $\Delta\sigma_S^D$ (mN m^{-1})	max. est. $\Delta\sigma_S^P$ (mN m^{-1})
	Min	Max			
Water	11.8	106.5	12.9	2.4	10.9
Ethylene Glycol	15.9	94.1	13.1	3.7	19.8
Glycerol	40.9	134.6	12.1	2.2	9.3
1-Bromon-aphthalene	7.9	47.0	6.9	2.1	—
Diio-domethane	17.5	57.1	5.1	1.9	—

4.4. Vibrational temperature

The resulting vibrational temperatures are presented in table 6 and the Boltzmann plot for maple and the CSBD, as an example, is shown in figure 9. The quality of the Boltzmann plot is indicated by the R^2 next to the determined temperatures in table 6. R^2 values next to 1 imply a linear behavior. Due to the R^2 of 0.94 or greater, a thermalized distribution can be suggested [39]. The vibrational temperatures show no significant dependence on the discharge type or the sample material according to the uncertainty of the fit, only slightly higher values for the CSBD and DDBD neglecting the accuracy of the method.

4.5. Electrical field strength and mean electron energy

The averaged values for the reduced electrical field strength, mean electron energy and mean electron temperature determined from comparing the simulated data with the measured ratios $R_{391/337}$, $R_{391/357}$ and $R_{391/380}$ are shown in table 7 with the corresponding standard derivations. They indicate no dependence on the material properties of density or moisture but a slight dependence on the power. As a result, there are higher variations for the CSBD and DDBD than for the RP. However, the power does not seem to be the only parameter as the high variations in the case of the DDBD show. Based on an assumed error of factor two in the method [40], all the data are equal.

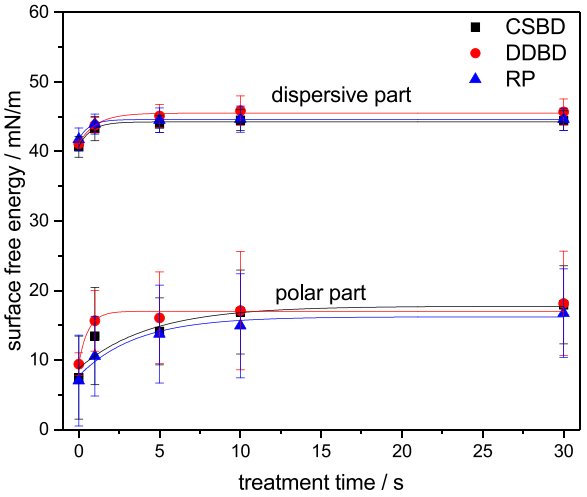

Figure 10. Surface free energy on maple depending on the plasma treatment time.

4.6. Contact angles and surface free energy

The contact angles of the five liquids show a significant reduction after the plasma treatment. By using liquids with different properties (table 3), the surface free energy can be calculated from the contact angles. Furthermore, the Fowkes model allows a distinction into a polar and dispersive part of the surface free energy. A rise of the surface free energies results from the reduction of contact angles.

Both the polar and dispersive part of the energy demonstrate an asymptotic behavior for all three materials (figures 10–12), except for the polar part on HDF. Here, a longer treatment time is necessary to indicate an asymptotic behavior.

For all parts—again, except the polar part on HDF—the largest increase is caused in the first seconds of the treatment time. A comparison of the three discharges shows nearly the same changes for the CSBD and DDBD and a slightly lower one for the RP. Thus, the efficiency of direct discharges, such as CSBD and DDBD, is higher than a jet system, such as RP. This difference is caused by a higher electron bombardment

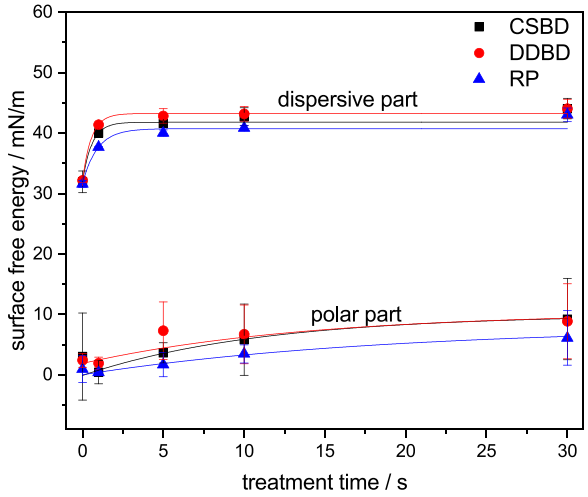

Figure 11. Surface free energy on HDF depending on the plasma treatment time.

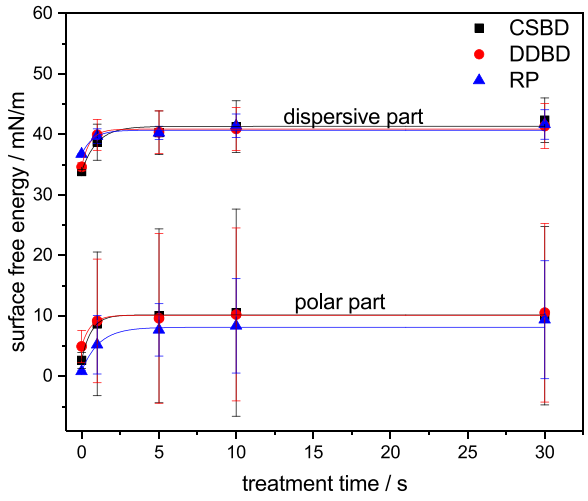

Figure 12. Surface free energy on WPC depending on the plasma treatment time.

and the production of reactive plasma species next to the surface.

Another discrepancy is the higher error of the polar part compared to the dispersive one. The reason for this is based on the calculation of the surface free energy and the error propagation. Table 8 shows a maximum error estimation. The higher errors of the polar part on WPC might be explained by a slightly lower treatment area and a sharp change of contact angle and therefore of the surface free energy.

The significant increase of the surface free energy indicates the possibility of changing the surface properties in the range defined by adhesives and coatings. Thus, especially on WPC, the adhesion of normal water-based wood coatings could be increased from less than 0.5 MPa to about 1 MPa for the CSBD and RP, and to 2 MPa for the DDBD.

5. Conclusion

The comparison of the three discharges shows only slight differences between the temperatures, the changes to the surface free energy and the reduced electrical field strength. The surface free energy—both parts on all materials—increases roughly asymptotic over the exposure time. The maximum changes are in the order of 10 mN m^{-1}, with smaller ones for the RP. Treatment times in the range of 1 s to 5 s prove to be the most efficient ones, due to the fast rise of the surface free energies. Only the polar part on HDF shows a significantly slower behavior, while its dispersive part increases more than on the other two materials. In summary, the CSBD and DDBD demonstrate the same efficiency, while the RP, due to its remote character, shows a slightly lower impact. Nevertheless, with the same setup and power, the choice of discharge is defined by the specific application. The CSBD without a grounded electrode below the material can be used for thick materials as wooden beams, as there is no limitation by the voltage range of the power supply. For materials of up to 1 cm thickness with slight variations in the thickness, a DDBD is the best choice. The RP, although a little less efficient, finds its application on materials with greater thickness and structures on the surface.

Acknowledgments

This work was funded by the Lower Saxony Ministry of Science and Culture and the German Federal Ministry of Education and Research (BMBF), under the supervision of Dr-Ing Karen Otten in Jülich, Germany, and the joint research project “PlaNaWood" (grant no. 03X5519B). Moreover, the authors would like to thank Robert Koslowski, HAWK Göttingen, for the infrared temperature measurements, Roger Skarsten, HAWK Göttingen, for proofreading, and Viktor Seifert for designing the setup.

ORCID iDs

F Peters https://orcid.org/0000-0001-6700-5138

References

[1] Yao Y, Liu X and Zhu Y 1993 *J. Adhes. Sci. Technol.* **7** 63–75
[2] Novák I and Florián Š 2001 *Polym. Int.* **50** 49–52
[3] Carrino L, Moroni G and Polini W 2002 *J. Mater. Process. Technol.* **121** 373–82
[4] Kikani P, Jain V, Nema S K, Visani A and Desai B 2015 *Surface Chemistry and Wettability Study of Air Plasma Treated Polyethylene by Atmospheric Pressure Dielectric Barrier Discharge* (https://doi.org/10.13140/RG.2.1.1026.0008)
[5] Risbrudt C D 2005 *Handbook of Wood Chemistry and Wood Composites* ed R M Rowell (Boca Raton, FL: CRC Press)
[6] Vioel W 2001 Method for modifying wooden surfaces by electrical discharges at atmospheric pressure *Patent* WO0139944
[7] Ibach R E 2005 *Handbook of Wood Chemistry and Wood Composites* ed R M Rowell (Boca Raton, FL: CRC Press)
[8] Rowell R M 2005 *Handbook of Wood Chemistry and Wood Composites* ed R M Rowell (Boca Raton, FL: CRC Press)
[9] Hill C A S 2006 *Wood Modification: Chemical, Thermal and Other Processes* (*Wiley Series in Renewable Resources*) (Chichester: Wiley)
[10] Wascher R, Leike N, Avramidis G, Wolkenhauer A, Militz H and Viöl W 2015 *Eur. J. Wood Wood Prod.* **73** 433–7

[11] Konnerth J, Weigl M, Gindl-Altmutter W, Avramidis G, Wolkenhauer A, Viöl W, Gilge M and Obersriebnig M 2014 *Holzforschung* **68** 707–12
[12] Avramidis G, Militz H, Avar I, Viöl W and Wolkenhauer A 2012 *Eur. J. Wood Wood Prod.* **70** 545–9
[13] Avramidis G, Nothnick E, Militz H, Viöl W and Wolkenhauer A 2011 *Eur. J. Wood Prod.* **69** 329–32
[14] Podgorski L, Chevet B, Onic L and Merlin A 2000 *Int. J. Adhes. Adhes.* **20** 103–11
[15] Podgorski L, Bousta C, Schambourg F, Maguin J and Chevet B 2002 *Pigment Resin Technol.* **31** 33–40
[16] Rehn P, Wolkenhauer A, Bente M, Förster S and Viöl W 2003 *Surf. Coat. Technol.* **174–5** 515–8
[17] Odrášková M, Ráhel' J, Zahoranová A, Tiňo R and Černák M 2008 *Plasma Chem. Plasma Process.* **28** 203–11
[18] Chelouah A, Marode E, Hartmann G and Achat S 1994 *J. Phys. D: Appl. Phys.* **27** 940–5
[19] Hünnekens B, Peters F, Avramidis G, Krause A, Militz H and Viöl W 2016 *J. Appl. Polym. Sci.* **133** 1097–4628
[20] Staack D, Farouk B, Gutsol A F and Fridman A A 2006 *Plasma Sources Sci. Technol.* **15** 818–27
[21] Laux C O 2002 *von Karman Institute Lecture Series* vol **7** (Rhode-Saint-Genèse, Belgium, 2002)
[22] Herzberg G W 1950 *Molecular Spectra and Molecular Structure* 2nd edn (New York: Van Nostrand)
[23] Mulliken R S 1958 *The Threshold of Space (Zelikoff, M.)* ed N Davidson pp 169–79
[24] Ochkin V N 2009 *Spectroscopy of Low Temperature Plasma* (Weinheim: Wiley)
[25] Gilmore F R, Laher R R and Espy P J 1992 *J. Phys. Chem. Ref. Data* **21** 1005
[26] Paris P, Aints M, Valk F, Plank T, Haljaste A, Kozlov K V and Wagner H E 2005 *J. Phys. D: Appl. Phys.* **38** 3894–9
[27] Pancheshnyi S 2006 *J. Phys. D: Appl. Phys.* **39** 1708–10
[28] Paris P, Aints M, Valk F, Plank T, Haljaste A, Kozlov K V and Wagner H E 2006 *J. Phys. D: Appl. Phys.* **39** 2636–9
[29] Hagelaar G J M and Pitchford L C 2005 *Plasma Sources Sci. Technol.* **14** 722–33
[30] Itikawa Y 2006 *J. Phys. Chem. Ref. Data* **35** 31–53
[31] Alves L L 2014 *J. Phys.: Conf. Ser.* **565** 012007
[32] Pancheshnyi S V, Sobakin S V, Starikovskaya S M and Starikovskii A Y 2000 *Plasma Phys. Rep.* **26** 1054–65
[33] Pancheshnyi S V, Starikovskaia S M and Starikovskii A 2000 *Chem. Phys.* **262** 349–57
[34] Pancheshnyi S V, Starikovskaia S M and Starikovskii A 1998 *Chem. Phys. Lett.* **294** 523–7
[35] Volpe C and Siboni S 1997 *J. Colloid Interface Sci.* **195** 121–36
[36] Rulison C 1999 So you want to measure surface energy? *Technical Note* 306
[37] Krüss GmbH 2002 *DSA1 v 1.80 Drop Shape Analysis: Manual V031008* (Hamburg: Krüss GmbH)
[38] Laux C O, Spence T G, Kruger C H and Zare R N 2003 *Plasma Sources Sci. Technol.* **12** 125
[39] Bruggeman P J, Sadeghi N, Schram D C and Linss V 2014 *Plasma Sources Sci. Technol.* **23** 023001
[40] Fantz U 2006 *Plasma Sources Sci. Technol.* **15** S137–47